Version of Record: https://www.sciencedirect.com/science/article/pii/S0142941820308709
Manuscript_ce28c41fe7a6ac22b4d615dd1b3d1075

Multiscale Structural Characterization of Biocompatible Poly(trimethylene carbonate) Networks Photo-cross-linked in a Solvent

Bas van Bochove

Polymer Technology, School of Chemical Engineering, Aalto University, Kemistintie 1, 02150 Espoo, Finland

Steve Spoljaric

ARC CoE in Convergent Bio-Nano Science and Technology, Department of Chemical and Biomolecular Engineering, The University of Melbourne, Grattan Street, Parkville 3010, Victoria, Australia

Jukka Seppälä

Polymer Technology, School of Chemical Engineering, Aalto University, Kemistintie 1, 02150 Espoo, Finland

Agustín Rios de Anda

Institut de Chimie et des Matériaux Paris-Est - Université Paris-Est Créteil, UMR 7182 CNRS, 2 rue Henri Dunant, 94320, Thiais, France

Abstract

Poly(trimethylene carbonate) (*PTMC*) polymeric networks are biocompatible materials with potential biomedical applications. By combining Dynamic Mechanical Analysis (DMA), Solid State Nuclear Magnetic Resonance (NMR), and tensile testing, it was possible to fully characterize the inner structure and its relationship with the macroscopic properties of photo-crosslinked *PTMC* materials in a solvent medium. *PTMC* prepared from macromer with various molecular weights (3 kg/mol, 18kg/mol, and 32 kg/mol) and with various polymer concentrations within the reactive media were analyzed, with the variation of thermomechanical properties and NMR signal decay characterized as a function of both aforementioned synthesis parameters. DMA and solid state Double Quantum (*DQ*) ^1H NMR investigations demonstrated that the network crosslink density is directly related to the macromer molar mass and polymer concentration. More interestingly, tensile tests confirmed that mechanical behavior depended on the materials' inner structure, notably their crosslink density. Specifically for the 18 kg/mol *PTMC* networks, dangling and free chains reinforced the network, exemplified by higher Young's modulus E values. This multiscale investigation provides a promising and precise approach to tailor the macroscopic behavior of *PTMC*

Email addresses: bas.vanbochove@aalto.fi (Bas van Bochove), rios@icmpe.cnrs.fr (Agustín Rios de Anda)

© 2020 published by Elsevier. This manuscript is made available under the CC BY NC user license
https://creativecommons.org/licenses/by-nc/4.0/

materials, by controlling their specific inner network structural morphologies during synthesis.

Keywords: Time-Domain ^1H *DQ* NMR, Dynamic Mechanical Analysis, Biocompatible polymers, Thermomechanical properties, Structure-properties relationship, Poly(trimethylene carbonate)

1. Introduction

Biodegradable polymer networks have great potential in biomedical applications due to their biocompatibility and biodegradability[1, 2, 3, 4, 5, 6, 7, 8, 9, 10, 11, 12, 13, 14, 15]. More specifically, tough elastomeric polymer networks are of interest as bulk materials[12, 16, 17, 18, 19, 20, 21]. Elastomeric polymer networks can be designed to exhibit mechanical properties required for their intended application, especially soft tissues[22]. Much work has been done to improve the toughness of the elastomeric networks, but it remains a challenge to obtain elastomers that are both degradable and tough[18].

To improve the toughness of elastomeric networks, the growth of micro-cracks must be hindered[23]. This has been extensively studied for both natural and synthetic elastomers, though many of these studies have been performed with non-degradable elastomers such as polyisoprene and poly(dimethyl siloxane) (PDMS)[24, 25, 26, 27, 28, 29]. The formation of micro-cracks in these networks was slowed down by introducing crystallizable domains into the polymer network, crosslinking in solvent, and crosslinking chains with bimodal chain length distributions.

Tough, biodegradable elastomeric networks have been prepared via the photo-crosslinking of methacrylate-functionalized *PTMC* oligomers (*PTMC* macromers) and acrylated poly(e- caprolactone-co-D,L-lactide) (P(CL-co-DLLA)) oligomers[16, 18, 30]. Such networks are formed by adding a photo-initiator which forms radical species upon light irradiation [31]. These radical species can initiate polymerization of the (meth)acrylate end-groups of the macromers, creating poly(methacrylate) kinetic chains as the networks are formed. In the case of *PTMC*-networks, toughness increased with macromer molecular weight[16]. In addition, the preparation of bimodal *PTMC* networks resulted in a significant increase in toughness[19]. For both *PTMC*- and *P(CL-co-DLLA)* macromers, crosslinking in solution resulted in less rigid networks that demonstrated increasing elongation with decreasing macromer concentrations, resulting in superior elastomer toughness[18, 30].

It has been suggested that the presence of solvent during crosslinking results in disentangled chains prior to crosslinking formation, which in turn leads to simpler topologies in the networks[25]. The crosslinks of such networks are more likely to be both spatial and topological neighbors as

compared to networks prepared in bulk. In addition, networks prepared in solution have fewer chain-junction and inter-chain entanglements. The polymer chains in these networks are less-firmly embedded in the network structure; subsequently these networks deform more non-affinely. In order to fully understand the influence of crosslinking in solution on the macroscopic properties of elastomeric networks, the thermomechanical behavior and structural morphology of these networks need to be fully studied.

To facilitate this, a macroscopic experimental approach combining tensile testing, DSC and DMA analyses, and Time Domain ^1H Double Quantum DQ NMR was undertaken in this work. Tensile tests yielded the macroscopic mechanical resistance of the studied $PTMC$ samples, while DSC and DMA allowed the evolution of molecular mobility to be analyzed via observation of the glass transition temperature. Moreover, DMA allowed the characterization of the mechanical crosslink density of $PTMC$ networks with varying molecular weight and solvent concentrations.[32, 33]. These studies were complemented by Time Domain ^1H DQ NMR. This specific technique has been principally used to characterize the structure, morphological organization and molecular mobility of polymeric networks [34, 35, 36, 37, 38, 39, 40, 41, 42, 43, 44, 45]. Double-Quantum DQ ^1H sequences have been proven to effectively characterize elastomeric-like polymer networks, specifically their molecular mobility, crosslink density v_C, and chain defect concentration w_{DEF}[46, 47, 48, 49, 50, 51, 52, 53, 54, 55, 56, 57], in addition to the evolution of these properties with temperature [58, 59], chemical [60, 61, 62] and physical modifications[63], and thermal ageing [64, 65]. This is made possible due to the ability of this technique to discriminate dynamical and structural effects, permitting semi-local structural features of networks to be recovered from local dynamical measurements.

More extensively, Time Domain ^1H DQ NMR has been efficiently used in combination with DMA analyses to study the relationship between the structure of $PTMC$ networks of various macromer molar masses, and their macroscopic thermomechanical behavior[66]. Therefore, this work is a logical evolution of this previous study. By applying the same approach to analyse the influence of polymer concentration during $PTMC$ network formation, we aim to deepen the understanding of the influence of intrinsic polymer structure on the macroscopic behavior of $PTMC$ networks, which in turn will provide deeper insight regarding how to chemically tailor network structure, so as to better regulate and adjust $PTMC$ specific macroscopic properties. $PTMC$ networks were chosen for this study, as such networks are extensively studied for a range of biomedical

applications requiring different properties, such as intervertebral disks [67], meniscus implants [17] and bone implants [20]. Its biocompatibility has been shown previously with, among others, synovium derived cells [68], mesenchymal stem cells [69], and chondrocytes [70] *in vitro* and in several studies *in vivo* [68, 71, 72].

2. Materials

Trimethylene carbonate (TMC) monomer was purchased from Huizhou ForYou Medical Devices Co. (China). Hydroquinone, methacrylic anhydride, tin(II) 2-ethylhexanoate ($Sn(Oct)_2$), Trimethylol propane (TMP), and triethylamine were purchased from Sigma (USA) and used as received. Dichloromethane and chloroform were obtained from Merck (Germany), and d-chloroform was purchased from VWR. Ethanol was obtained from Altia oyj (Finland). TPO-L (2,4,6-trimethylbenzoylphenyl phosphinate) was obtained from Carbosynth Limited (United Kingdom).

2.1. Macromer Synthesis

To obtain star-shaped methacrylate-functionalized *PTMC* oligomers (macromers), hydroxyl-terminated *PTMC* oligomers were first prepared by ring-opening polymerization reactions of TMC at 130 °C under a nitrogen atmosphere for 3 days using TMP as initiator and $Sn(Oct)_2$ as catalyst. Oligomers with different molecular weights ($\overline{M_n}$) could be prepared by adjusting the monomer-to-initiator molar ratio. Second, the oligomers were dissolved in dichloromethane (2 mL/g oligomer) and functionalized with methacrylic anhydride (7.5 mol/mol oligomer) in the presence of triethylamine (7.5 mol/mol oligomer). Hydroquinone (0.1 wt% relative to the monomer) was added to the solution to act as a free-radical scavenger to prevent premature crosslinking. The macromers (*PTMC-tMA*) were precipitated in cold ethanol after 5 days and dried at 40 °C under vacuum for 1 week. The $\overline{M_n}$ of the obtained oligomers, the monomer conversion, and the degree of functionalization were determined by ^{1}H-NMR as described previously.[17] Briefly, the molecular weight was determined by comparing the area of the $-CH_3$ group of the initiator peak at $\delta = 0.92$ ppm with the area of the *PTMC* methylene peak at $\delta = 4.24$ ppm. The conversion was calculated by comparing the area of the *PTMC* methylene peak at $\delta = 4.24$ ppm with the area of the TMC monomer peak at $\delta = 4.45$ ppm. The degree of functionalization was determined by comparing the $-C{=}CH_2$ ^{1}H signals at $\delta = 5.58$ ppm and $\delta = 6.13$ ppm of the methacrylate groups with the $-CH_3$ initiator peak.

2.2. Network Formation

To photo-crosslink *PTMC* in bulk (also called 100% hereafter), the macromers were dissolved in chloroform and 5 wt% TPO-L photo-initiator (relative to the macromer) was added. The solutions were cast in teflon molds and kept in the dark overnight to allow for chloroform evaporation.

To photo-crosslink *PTMC* in solution, the macromers were dissolved in propylene carbonate at 70 °C. The polymer solutions contained 87.5, 75, 62.5, 50 or 40 wt% polymer. After complete dissolution, 5 wt% TPO-L photo-initiator (relative to the macromer) was added to the solutions. The solutions were cast onto a glass plate to obtain networks with an approximate thickness of 1 mm.

The cast macromers were crosslinked at room temperature under nitrogen in a custom built cross-link box for 30 min at 395-405 nm at an intensity of 1 mW/cm^2. The obtained networks were subsequently post-cured under visible light for 40 min at room temperature. The conversion of the $-C{=}CH_2$ double bond was confirmed by ATR-IR (Spectrum Two, Perkin Elmer). As these networks have a functionality f=3, the theoretical chemical cross-link density v_{chem} of such networks can be calculated as $1/3\overline{M_n}$.

3. Experimental Methods

3.1. Swelling Characterization

The volume degree of swelling q was determined in triplicate at room temperature by swelling rectangular shaped specimens (5×5×1 mm^3) in chloroform for 24 h, which was sufficient time to reach solvent sorption equilibrium. The q was calculated from Equation 1

$$q = 1 + \left(\frac{m_{swollen} - m_{dry}}{m_{dry}}\right)\left(\frac{\rho_p}{\rho_s}\right) \tag{1}$$

where $m_{swollen}$ is the mass of the swollen networks, m_{dry} the mass of the networks after drying, and ρ_p and ρ_s the densities of *PTMC* (=1.31 g/cm^3)[16] and chloroform (=1.48 g/cm^3), respectively.

3.2. DSC Analysis

The thermal properties of the obtained *PTMC* networks were determined by a TA Instruments Q2000 differential scanning calorimetry (DSC). Samples with weights between 5 and 10 mg were cooled to -90 °C and subsequently heated to 100 °C at 10 °C/min. After a second cooling cycle

to -90 °C at 10 °C/min the samples were held at -90 °C for 5 min and a second heating scan was performed. The glass transition temperatures (T_g) were determined from the second heating scan. Temperature calibration was performed using indium as a calibration standard.

3.3. Tensile experiments

The tensile properties of the networks were determined by tensile testing using an Instron universal tensile tester 5944, equipped with a 2 kN load cell at 24 °C and 50% relative humidity. The tensile samples dimensions were 5.3×40 mm^2. The elongation of the samples was determined from the grip-to-grip separation which was initially 20mm. The tensile modulus (E), maximum tensile strength (σ_{max}) and elongation at break (ε_{break}) were determined according to ASTM D882 at a test speed of 10mm/min. The yield stress (σ_{yield}) and elongation at yield (ε_{yield}) were determined from the intersection of the tangents to the stress strain curve. The toughness (W) was determined by calculating the area under the stress-strain curve. Five specimens of each type of network were used for the tensile testing.

3.4. Dynamic Mechanical Analysis

Dynamic Mechanical Analyses were performed using a TA Instruments Q800 DMA operating in tensile mode. *PTMC* samples were cut into ISO 527-4b dogbone-shaped specimens with dimensions of $18 \times 2 \times 0.7 mm^3$. Samples were heated from -140°C to 150°C with a heating rate of 3°C/min under a frequency of 1 Hz, a pre-strain of 0.01%, and a subsequent strain of 0.1%. The main α relaxation temperature T_α was calculated from the half-height point of E' drop corresponding to this relaxation [73]. All values are shown as averages ± standard deviation of 5 repeats.

Furthermore, the crosslinking density v_{C-DMA} for each *PTMC* network was obtained by conducting a DMA strain sweep measurement at T_α + 90°C so as to allow a precise comparison between these results and those obtained by NMR at the same molecular mobility state. The linear regime was thus determined by plotting the storage modulus E' as a function of the strain ϵ and the value of E' was taken from the linear regime plateau. Then, the crosslinking density v_{C-DMA} was calculated according to Equation 2[32].

$$v_{C-DMA} = \frac{E'}{\phi RTf} \tag{2}$$

where R is the ideal gas constant = 8.314 $J/mol \cdot K$, T=T_α + 90°C, f is the network functionality which for *PTMC* samples is equal to 3, and ϕ is a factor linked to the network model. For

the *affine* model[74] $\phi = 1$, whereas for the *phantom* model [75] $\phi = \frac{f-2}{f}$. In this work, two series of v_{C-DMA} values were thus calculated according to both the affine and phantom models.

3.5. DQ ^1H Solid State NMR Measurements

^1H Double Quanta *DQ* experiments were conducted on a Bruker Avance III 400 NMR equipped with a 5mm ^1H Static probe. These experiments are based on Baum - Pines pulse sequences[47, 48] optimized by Saalwächter[49, 50, 51, 52, 53, 56, 54, 57, 58, 59, 65]. Such experiments yield two components as a function of the *DQ* evolution time τ_{DQ} : the DQ buildup I_{DQ} and the reference decay I_{REF}. Figure SI.1 (*Support Information*) shows an example of such signals. The full magnetization of the sample I_{TOT} corresponds to the sum of I_{DQ} and I_{REF}, and comprises the response of both the dipolar coupled network and the uncoupled mobile network defects such as dangling or free chains. These fractions are characterized by different types of relaxation behavior. Chains fully belonging to the network relax faster and non-exponentially, whereas dangling and free (*i.e.* non-elastic) chains exhibit a slower exponential relaxation.

As described previously[66], in order to properly get access to the network structure, *DQ* experiments must be undertaken in the temperature-independent regime, *i.e.* the probed molecular motions must be effective in the fast motion regime. Preliminary studies on *Bulk 3k PTMC* were carried out at various temperatures ranging from T_α + 50 C° to T_α + 100 C°. Such measurements showed that the temperature-independent was reached for T_α + 90 °C (see Equation SI.1 and Figure SI.2 (*Support Information*). In this work, all of the samples were thus studied at $T = T_\alpha$ + 90 °C, ensuring that they were all tested at the same state of molecular mobility in the temperature-independent regime of the *DQ* signal.

In this temperature-independent regime, to discriminate the network structure influence on the *DQ* build-up, a normalization of this signal has to be carried out. This normalized signal I_{nDQ} is calculated according to Equation 3 and theoretically it must reach a plateau at the value 0.5[62, 76].

$$I_{nDQ} = \frac{I_{DQ}}{I_{REF} + I_{DQ} - I_{DEF}} \tag{3}$$

This normalization (*i.e.* Equation 3) considers the subtraction of the non-elastic chains I_{DEF} (*i.e.* dangling or free chains) contribution from the total signal. A heuristic approach readily allowing the identification and subtraction of this contribution is to fit I_{DEF} through a double exponential from the $I_{REF} - I_{DQ}$ *v.s.* τ_{DQ} signal [53, 62]. Extrapolating this I_{DEF} fit to $\tau_{DQ} = 0$

gives the percentage of defects (*i.e.* non-elastic chains) w_{DEF}. An example of this approach is given in Figure SI.1 (*Support Information*).

DQ NMR experiments give access to the dipolar coupling constant D_{res}, which is related to an average local dynamic segmental orientation parameter. D_{res} is in turn related to the crosslink density ν_C through Equation 4:

$$v_C \propto \frac{1}{M_C} \propto k\frac{D_{res}}{D_{stat}} \tag{4}$$

where D_{stat} is the static dipolar coupling constant and k a proportionality factor related to the details of intersegmental motions at the scale of the Kuhn length. Then, the numerical value of D_{res}, related to the network structure, is obtained by fitting the corresponding I_{nDQ} signal up to 0.48 by Equation 5 (See Figure SI.3 - *Support Information*).

$$I_{nDQ} = 0.5\,[1 - exp\,(-D_{res}\tau_{DQ})^n] \tag{5}$$

where n is an exponent varying between 1 and 2. The closer n is to the value of 2, the more homogeneous the networks are. In this investigation, the values for k and D_{stat} were not obtained, nevertheless these factors should be identical for all samples. Thus, a quantitative comparison between all studied materials can be performed as described in Equation 4 by obtaining D_{res}.

4. Results and discussion

Three-armed *PTMC* macromers were synthesized via the ring-opening polymerization of *TMC* into *PTMC* oligomers followed by functionalization with methacrylic anhydride. By adjusting the monomer-to-initiator ratio, oligomers with three different molecular weights were obtained. Table 1 shows the obtained oligomer molecular weights as confirmed by ^{1}H-NMR. The subsequent functionalization resulted in macromers with a degree of functionalization of ≥ 86 %. In Figure SI.4 (Support Information), a typical ^{1}H-NMR spectra of a *PTMC* oligomer and macromer is shown. Detailed interpretations of such spectra can be found elsewhere[16]. The chemical structure of the *PTMC* macromer is shown in Figure 1.

PTMC networks were prepared by solvent casting and subsequent photo-crosslinking resins containing 6 different concentrations of polymer. For the two highest molecular weights, some polymer concentrations were too viscous to be cast, even though the resins were heated to 70 °C. The conversion of the $-C{=}CH_2$ double bond was confirmed by ATR-IR. The methacrylate double

Table 1: Conversion and Degree of Functionalization of the Obtained *PTMC* Macromers

M_n (g/mol)	Conversion (%)	Degree of Functionalization (%)
3100 (*3k*)	97	100
18000 (*18k*)	99	100
32400 (*32k*)	97	86

bond (1640 cm^{-1}) disappears when it polymerizes during the photo-crosslinking, as can be seen in Figure 2. The obtained networks were extracted and dried prior to characterization.

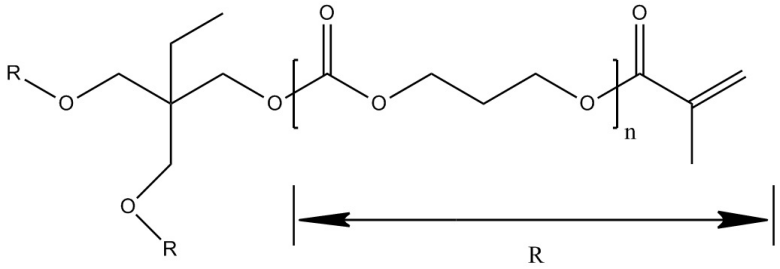

Figure 1: Chemical structure of *PTMC* macromer.

The glass transition temperatures T_g of the obtained networks were determined by DSC and are shown in Table 3. The trend in the T_g values of the networks is similar to that observed by Schüller et al[16]: with increased macromer molecular weight the, T_g decreases. While slight differences can be observed between the solvent-cast networks prepared with the same molecular weight macromers, no correlation between the obtained T_g values and polymer concentration during cross-linking is observed. In addition, Table 3 shows that the degree of swelling q increased not only with macromer molecular weight, but also with decreasing polymer content. This indicates that when cross-linking in the presence of solvent, the cross-link density seems to decrease with polymer concentration.

Zant et al. previously demonstrated that the elongation, and thus the toughness, of extracted and dried *PTMC* networks prepared from two-armed *PTMC* macromers with a molecular weight of 10 kg/mol was strongly dependant on the amount of solvent present at the time of crosslinking [18]. Decreasing the polymer concentration within the reactive media resulted in the elongation and toughness significantly increasing. We expected this to be the same for our extracted and dried networks prepared from three armed macromers, as it was previously shown that by decreasing the

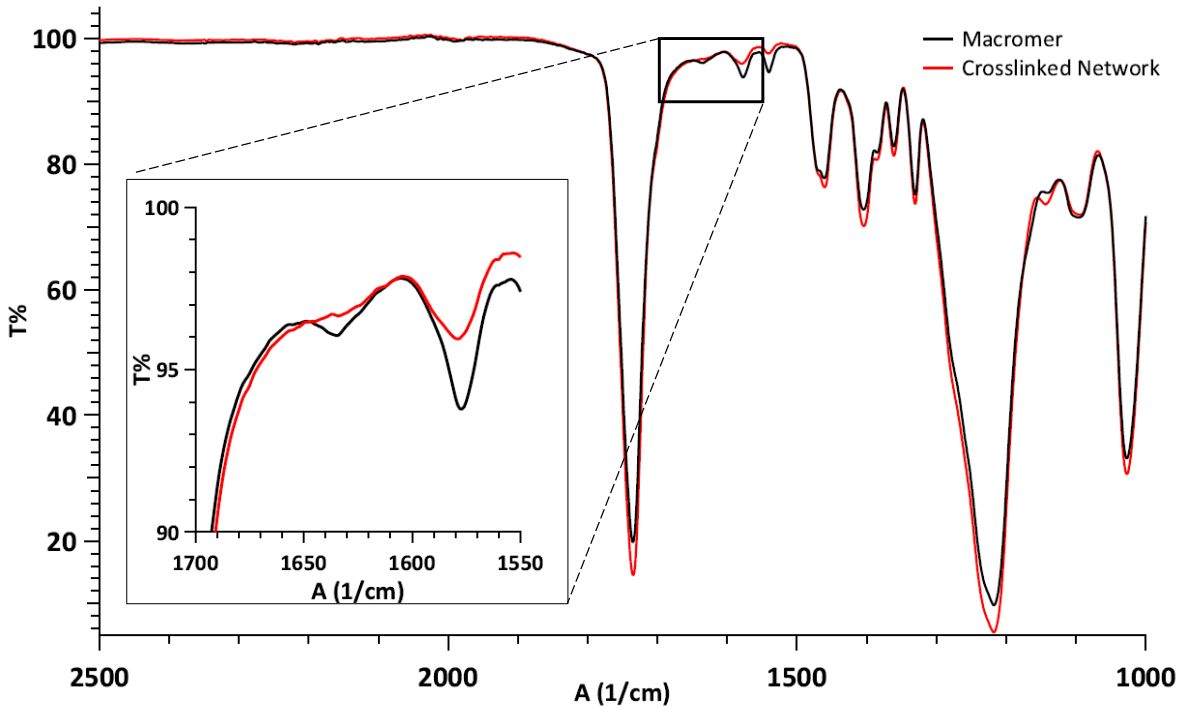

Figure 2: Typical IR spectra of a *PTMC* macromer and its subsequently obtained network. The insert shows the disappearance of the methacrylate double bond at 1640 cm^{-1} which occurs due to the photo-crosslinking.

network density by means of increasing the three-armed macromer molecular weight, the elongation and toughness of the networks was increased [66, 16]. And as shown above, our networks exhibited a decrease in network density with decreasing polymer content. To confirm this, five samples per network were cut from the network films and subjected to tensile testing. An overview of the results can be found in Table 2.

Indeed, within each molecular weight, the elongation at break increases with decreasing polymer concentration. Figure 3a illustrates this trend showing typical stress-strain curves of *PTMC 3k* networks. Figure 3b further highlights this trend for all networks within this study. The toughness of the networks generally increases with decreasing macromer content, except for networks prepared from the two lowest polymer concentrations which utilized macromers with a molecular weight of *3k*; this is shown in Figure 3c. It appears that the considerable decrease of modulus for these two networks results in a decrease in toughness. The networks prepared from *PTMC 3k* are the only networks that show such a considerable decrease in modulus through the series. as exemplified in Figure 3d.

DMA analyses yielded the main transition temperature T_α as well as the elastic modulus E' at T_α+90°C for each *PTMC* sample. These values are listed in Table 3. From these values

Mn (g/mol)	$Polymer$ (wt%)	$E-modulus$ (MPa)	σ_{yield} (N/mm^2)	σ_{max} (N/mm^2)	ε_{yield} (%)	ε_{break} (%)	W (N/mm^2)
3k	100	12.2 ± 0.49	1.38 ± 0.23	3.19 ± 0.42	12.4 ± 2.75	42.0 ± 7.83	77.3 ± 21.7
	87.5	11.6 ± 0.54	1.47 ± 0.40	4.20 ± 0.76	13.8 ± 4.54	66.2 ± 12.6	158 ± 44.7
	75	8.50 ± 0.92	1.04 ± 0.26	3.68 ± 0.91	13.7 ± 3.76	81.4 ± 18.7	170 ± 79.2
	62.5	6.27 ± 1.37	1.03 ± 0.15	4.26 ± 1.01	17.7 ± 5.75	154 ± 26.6	370 ± 131
	50	4.13 ± 0.81	0.78 ± 0.19	3.27 ± 0.62	20.7 ± 9.99	181 ± 33.9	338 ± 114
	40	2.45 ± 0.63	0.63 ± 0.08	2.20 ± 0.24	30.5 ± 11.0	196 ± 14.4	237 ± 34.1
18k	100	2.45 ± 0.22	0.86 ± 0.14	1.47 ± 0.24	39.1 ± 7.73	137 ± 24.2	127 ± 42.7
	62.5	3.98 ± 0.58	0.92 ± 0.12	1.92 ± 0.38	23.3 ± 1.21	213 ± 63.0	270 ± 118
	50	3.34 ± 0.51	0.95 ± 0.13	1.64 ± 0.31	29.5 ± 4.43	230 ± 27.3	262 ± 82.3
	40	2.86 ± 0.65	0.85 ± 0.06	2.19 ± 0.15	32.1 ± 11.4	609 ± 63.5	877 ± 157
32k	100	3.12 ± 0.30	1.03 ± 0.14	2.53 ± 0.42	35.3 ± 5.74	504 ± 26.9	849 ± 95.5
	50	2.62 ± 0.19	1.17 ± 0.10	1.93 ± 0.22	47.7 ± 3.62	716 ± 47.8	1051 ± 119
	40	2.57 ± 0.19	1.12 ± 0.16	1.72 ± 0.28	48.4 ± 5.09	868 ± 65.4	1221 ± 240

Table 2: Tensile properties of the studied *PTMC* networks.

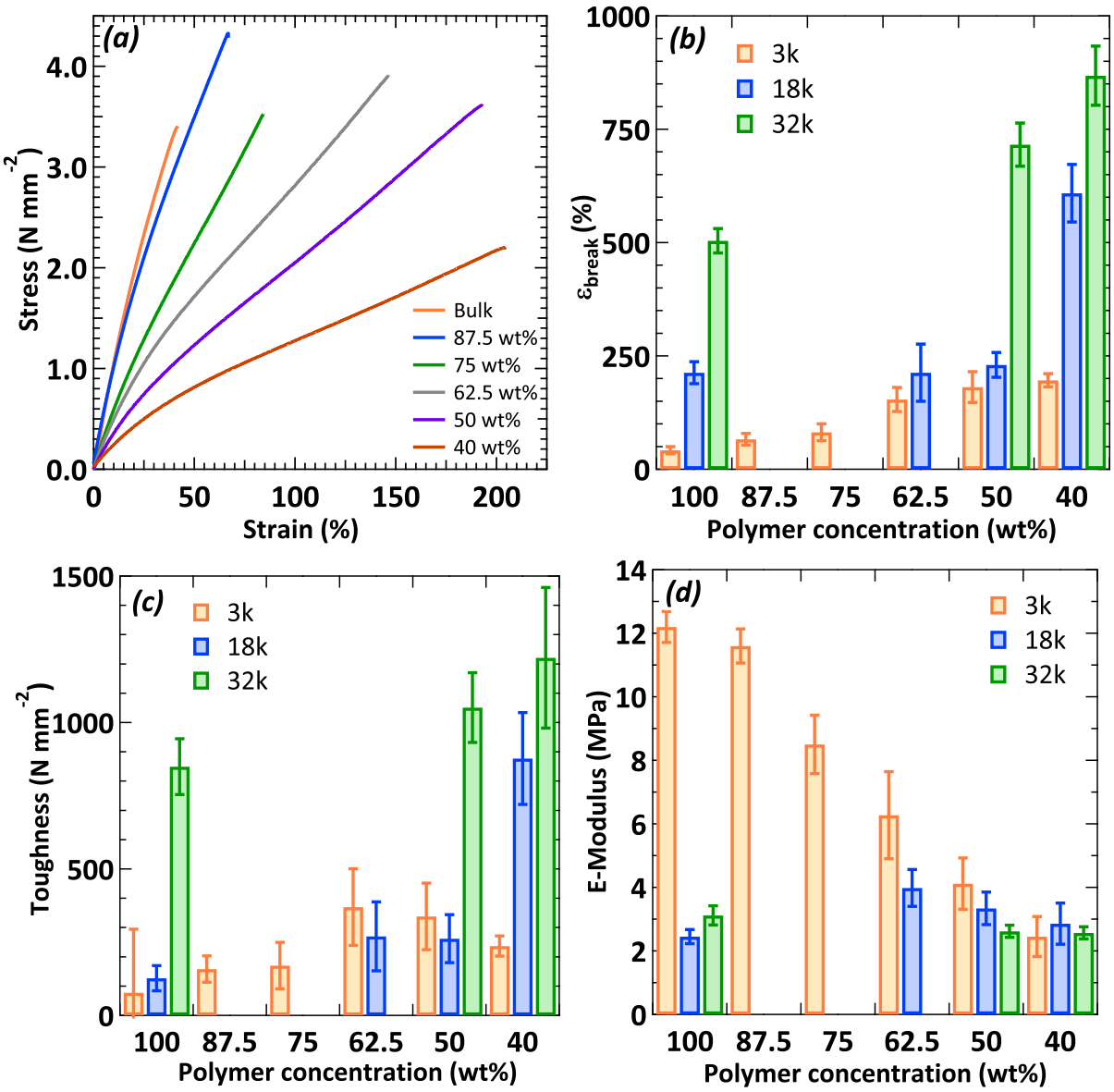

Figure 3: Overview of the tensilte testing results of the extracted and dried *PTMC* networks. (a) Typical stress-strain curves of solvent-cast networks prepared from *PTMC 3k* macromer with different polymer contents. Trends in the change of (b) the strain at break, (c) the toughness, and (d) of the Young's E modulus as a result of changing the polymer content.

the crosslink densities ν_C were calculated using Equation 2 according to the *affine* and *phantom* models. The computed values for all samples are also listed in Table 3.

Subsequently, I_{nDQ} signals normalized according to Equation 3 were obtained by DQ ^1H NMR. Figure 4a plots the obtained I_{nDQ} signals for *Bulk PTMC 3k*, *18k* and *32k* samples. It is observed that the I_{nDQ} signal becomes steeper when the macromer mass increases, which can be linked to an increase in crosslink density ν_C. These signals were then fitted by Equation 5 in order to obtain the D_{res} value for each sample, which are listed in Table 3. Figure 4b plots the same I_{nDQ} signals as a function of the normalized DQ time $D_{res}\tau_{DQ}$. It is seen that all I_{nDQ} signals superpose, which would mean that the chemical and physical network structure for the three *Bulk PTMC* networks is the same. This has been previously observed for such materials[66].

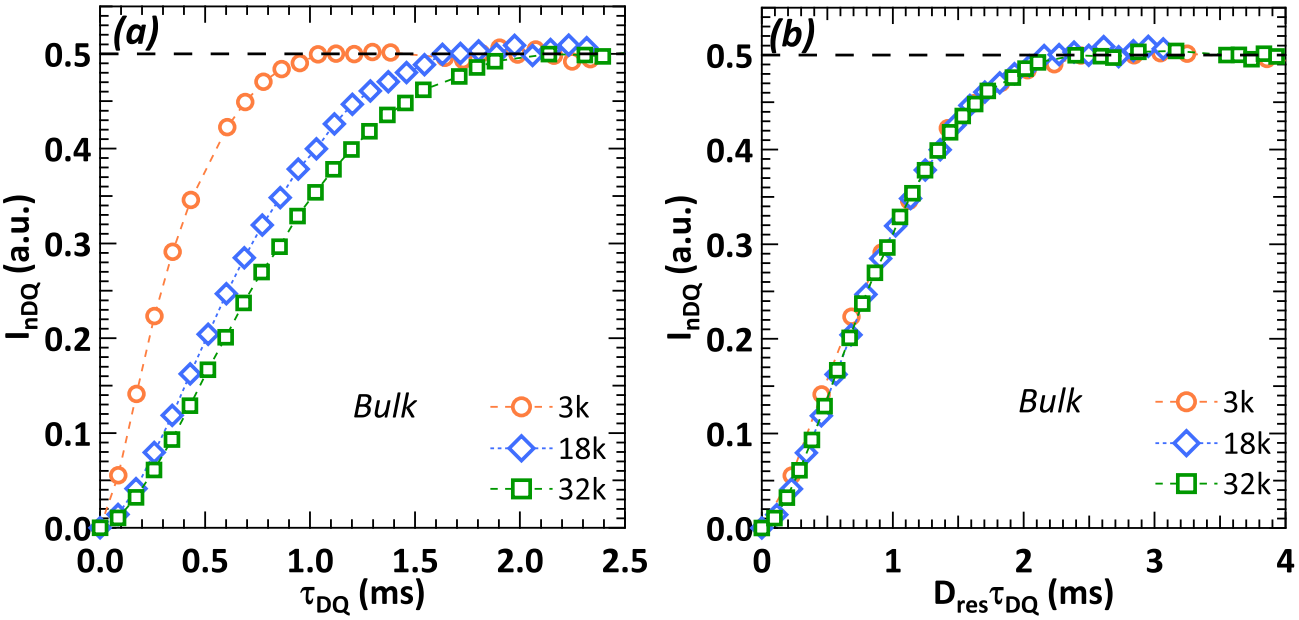

Figure 4: (a) I_{nDQ} values as a function of τ_{DQ} for *Bulk PTMC* networks obtained by DQ ^1H NMR at T_α + 90 °C. (b) Same plot with a normalization of τ_{DQ} by D_{res}.

The same approach was undertaken for solvent-cast *PTMC* networks. Figure 5 shows the I_{nDQ} signals obtained for the *3k*(a), *18k*(c), and *32k*(e), solvent-cast *PTMC* networks with varying polymer concentration. For each macromer molecular weight (*i.e. 3k*, *18k*, and *32k*) it is systematically seen that when the polymer content increases, the I_{nDQ} signal becomes steeper. This is expected as propylene carbonate would act as a spacer between macromer chains, hindering the formation of denser crosslink networks. Thus, it can be concluded that the networks crosslink density strongly depends on the polymer content in the reactive medium.

Table 3: Physico-chemical, DSC, DMA, and ^1H *DQ* NMR results obtained for the studied *PTMC* networks.

PTMC	Polymer	Physico-chemical		DSC	DMA				MQ ^1H NMR		
		q	ν_{C-chem}	T_g	T_α	E' @ $T_\alpha + 90°C$	ν_{C-DMA} affine	ν_{C-DMA} phantom	$D_{res}/2\pi$	w_{DEF}	n
	($wt\%$)		(mol/g) $\times 10^4$	(°C)	(°C)	(MPa)	(mol/g) $\times 10^4$		(Hz)	(%)	
3k	100	4.36 ± 0.55	8.82	-5.1	-11.7	9.1	10.32	30.95	359.7	4.3	1.46
	87.5	6.33 ± 0.50		-3.2	-12.5	7.3	8.35	25.06	335.6	1.6	1.52
	75	5.53 ± 0.08		-4.2	-12.9	4.8	5.49	16.46	294.7	3.4	1.58
	62.5	5.53 ± 0.03		-4.1	-12.4	4.0	4.56	13.67	262.3	5.3	1.56
	50	7.30 ± 0.57		-5.5	-12.4	2.6	2.95	8.85	236.9	5.2	1.59
	40	8.05 ± 0.33		-4.9	-13.2	1.9	2.21	6.63	223.7	1.2	1.80
18k	100	8.71 ± 0.20	1.80	-11.8	-20.4	4.8	5.62	16.85	210.5	1.2	1.70
	62.5	9.72 ± 0.12		-11.9	-22.5	4.4	5.19	15.56	200.3	2.5	1.79
	50	12.9 ± 0.57		-11.9	-21.8	2.8	3.30	9.91	191.2	4.6	1.76
	40	15.2 ± 0.44		-12.0	-22.1	1.0	1.21	3.63	160.8	6.0	1.72
32k	100	10.3 ± 0.51	1.04	-12.4	-14.8	4.4	5.09	15.28	178.5	13.8	1.70
	50	15.3 ± 1.45		-13.7	-20.7	2.8	3.23	9.68	169.7	4.9	1.78
	40	22.6 ± 0.14		-13.1	-21.7	2.3	2.66	7.97	161.8	3.9	1.77

Then, I_{nDQ} signals were fitted by Equation 5, yielding the numerical value of D_{res} for each solvent-cast sample, which are summarized in Table 3. Figures 5b, 5d, and 5f represent these I_{nDQ} signals as a function of the normalized time $D_{res}\tau_{DQ}$. Once more, for a given macromer molar weight, all I_{nDQ} signals superpose with each other with this normalization, implying that although the crosslink density ν_C depends on polymer concentration during *PTMC* crosslinking, the chemical and physical morphology of the solvent-cast *PTMC* networks remains the same regardless of macromer molecular weight and initial polymer concentration.

Furthermore, for all bulk and solvent-cast *PTMC* networks, the D_{res} values obtained by *DQ* ^1H NMR were plotted as a function of the crosslink density ν_C calculated by the phantom model from DMA data as shown in Figure 6. (A similar plot with ν_C calculated from the affine model is shown in Figure SI.5 - *Support Information.*)

Figure 6 shows that for each macromer molecular weight, a systematic linear relationship between D_{res} and ν_C is obtained with a non-zero intercept for $v_C = 0$. This linear relationship is expected from rubber elasticity theory[77, 78] as well as from the affine[74] and phantom[75] models. Analogous results have been observed in elastomers[62] as well as in *PTMC Bulk* for networks of various molecular weights[66]. From this plot, several phenomena and conclusions can be drawn.

First of all, the non-zero intercept corresponds to physical entanglements within the networks. As mentioned in[66], *DQ* ^1H NMR is able to probe these entanglements as they relax in a time domain slower or similar to those of the experiment, contrary to DMA whose characteristic measuring time is longer, during which entangled chains have relaxed. Moreover, it is observed in Figure 6 that the non-zero intercept value for *PTMC* networks diminishes with macromer molar weight (*i.e.* $D_{res-0-3k} = 191.1Hz$, $D_{res-0-18k} = 150.9Hz$, and $D_{res-0-32k} = 147.0Hz$). This may be attributed to a higher probed crosslink density induced by shorter macromer chains. Furthermore the D_{res-0} values for 18k and 32k are close to those reported in our previous work[66] ($D_{res-0} = 135.5Hz$) in which a *PTMC 40k* network had the largest molecular weight. These values are relatively high when compared to the D_{res} values for *Bulk PTMC*. This would mean that the presence of physical entanglements contributes significantly to network properties, especially for low polymer content and/or high macromer molecular weight. This is especially true for the *32k PTMC* network, where the variation of D_{res} with polymer concentration is small.

Moreover, the D_{res} *vs.* ν_C slopes diminish with increasing macromer molecular weight. The

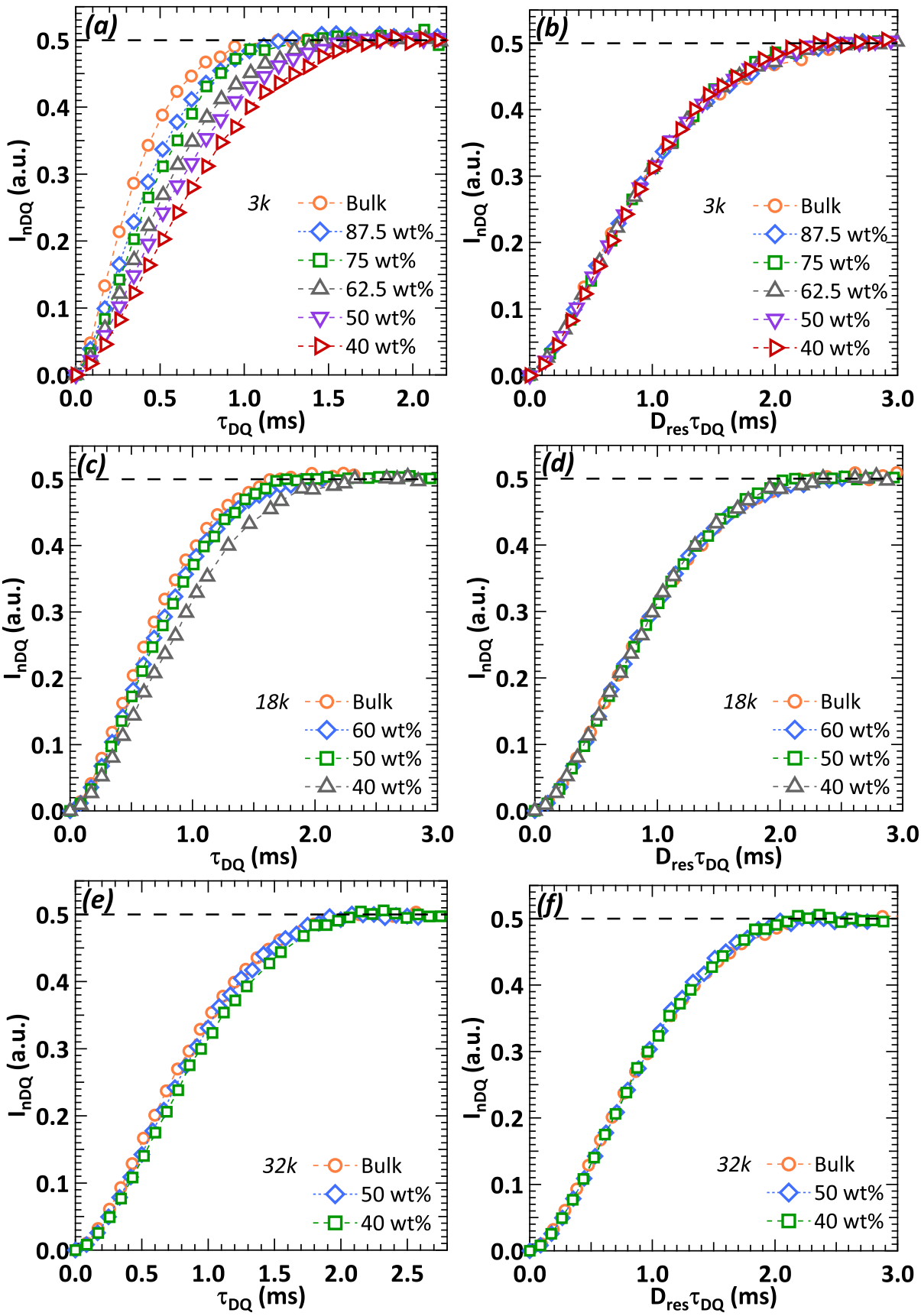

Figure 5: I_{nDQ} values as a function of τ_{DQ} for (a) 3k (c) 18k, and (e) 32k solvent-cast *PTMC* networks obtained by *DQ* ^1H NMR at T_α + 90 °C. (b,d,f) Same plots with a normalization of τ_{DQ} by D_{res}. The percentages correspond to polymer content in the reactive media.

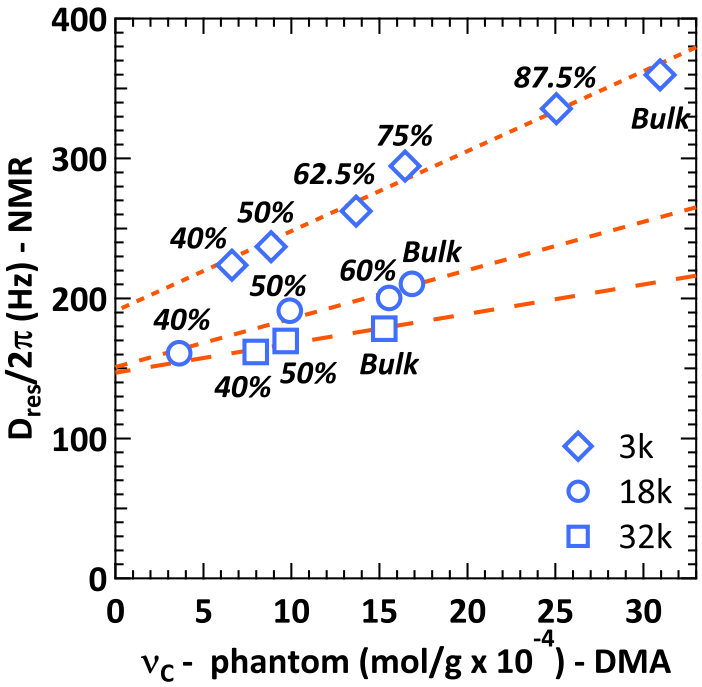

Figure 6: D_{res} values obtained by $DQ\ ^1H$ NMR measurements as a function of DMA ν_C crosslink densities calculated from the *phantom* model for all studied *Bulk* and *Solvent-cast PTMC* networks. Percentages correspond to polymer content in the reactive media. Dashed lines are linear fits and act as a guide for the eyes.

$DQ\ ^1H$ NMR data indicates that the influence of polymer concentration on the *chemical* crosslink density decreases as macromer molecular weight increases. This is expected because the crosslink density of the bulk networks decreases with increasing molecular weight, therefore solvent molecules would diffuse easily between two macromer reactive functionalities, limiting its steric influence.

Additionly, the $DQ\ ^1H$ NMR analyses yielded the percentage of defects w_{DEF} and *"network homogeneity factor"* n (*i.e.* Equation 5). These values are compiled in Table 3. In the case of the n factor, it was systematically observed that for all macromer molecular weights, that when the polymer concentration decreases, n gets closer to the value of 2 (*i.e.* a *"homogeneously crosslinked"* network). This could be explained by the following hypothesis: as *propylene carbonate* acts as a spacer during the crosslinking reaction, *PTMC* macromer chains are less constrained and entangled within the reactive mixture. This would enahnce the efficiency and likelihood of steric-oriented reactions between macromers, inducing a better-ordered network following photocrosslinking.

Furthermore, the evolution of the percentage of defects w_{DEF} with polymer concentration seems to depend on the macromer molecular weight. Indeed, each *PTMC* series of networks have a different evolution of w_{DEF} with polymer content, as can be seen from the values reported in

Table 3. In the case of *PTMC 3k* networks, no clear evolution of w_{DEF} is observed, with the values remaining close to each other. This could be explained by the fact that macromer chains are relatively short. Indeed, *PTMC* repeating unit molar mass is M_0=102 g/mol, so the *3k* network possesses *ca.* 30 repeating units per chain (which is only *ca.* 10 repeating units per arm). Even though a better-ordered network is obtained, dangling or free chains are still obtained due to some steric hindrance as a result of the size of the macromer chain. Concerning the *PTMC 18k* networks, it is seen in Table 3 that w_{DEF} increases with decreasing polymer content. The *18k* network possesses ca. 150 repeating units per chain (*ca.* 50 repeating units per arm). It is probable that *propylene carbonate* induces some steric hindrance in the reactive medium, hampering crosslinking reactions, generating a higher amount of dangling and free chains. Lastly, for the *PTMC 32k* networks, Table 3 shows that w_{DEF} decreases with polymer concentration, contrary to the *PTMC 18k* networks. The *32k* network possesses ca. 300 repeating units per chain (*ca.* 100 repeating units per arm). In this case, it is possible that less steric hindrance is induced by the presence of *propylene carbonate*, allowing more crosslink reactions, thus yielding a lower amount of defects.

Finally, it would seem that the percentage of defects w_{DEF} has a prominent influence on *PTMC* macroscopic properties. As expected, material toughness and elongation at break depended mainly on the crosslink density as previously shown in Figure 3. However, in the case of the measured Young's modulus E, its evolution with the *PTMC* structural morphology is more complex. It would also be expected that E would primarily depend on the crosslink density. Nonetheless, in the case of *PTMC 18k*, E increases when the polymer concentration decreases (*i.e.* when the crosslink density decreases). However, for this macromer molecular weight, the percentage of defects w_{DEF} increased when the polymer content decreased (*i.e.* Table 3). This would mean that for this given macromer molecular weight, *dangling and free chains seem to mechanically reinforce the materials.* In the case of *PTMC 3k* and *32k*, w_{DEF} remains constant or increases with polymer content, as does E. This indicates that dangling or free chains play a less important role in determining the mechanical moduli when compared to the influence of the polymer's crosslink density.

5. Conclusion

This investigation has highlighted the advantages of combining a multiscale experimental approach to better understand the macroscopic mechanical properties of *PTMC* networks from their intrinsic structural morphology. By combining tensile testing, DMA analyses and ^1H *DQ* NMR

measurements it was shown that *PTMC* crosslink density depended on the polymer content during the crosslinking reaction; the lower the polymer content, the lower the crosslink density value. This was systematically observed for the three studied macromer molar masses of *3k*, *18k* and *32k*. Moreover, it was observed by ^{1}H *DQ* NMR that even though the samples had varying crosslink densities, their intrinsic chemical and physical network morphology remained the same. Furthermore, it was observed that *PTMC* becomes more ductile (*i.e.* a decrease in toughness and an increase in elongation at break) when the polymer content decreases, *ergo* the crosslink density decreases. More surprisingly, it was observed that for the *PTMC 18k*, an increase in Young's modulus E was observed when the polymer content decreased (*i.e.* decrease of crosslink density). Indeed, for the *PTMC 3k* and *32k*, E diminished when the polymer content decreased, which is expected as fewer chemical or physical crosslinks are present in the material. In the case of *PTMC 18k*, the rise of E might be due to the presence of a higher amount of dangling and free chains acting as reinforcement. A higher percentage of dangling and free chains is attributed to *propylene carbonate* hampering crosslinking reactions due to steric hindrance. With this study, the understanding of how the chemical and structural tailoring of *PTMC* networks influences macroscopic properties has been deepened. This proven approach will be applied to study the network structure and functional macroscopic properties of heterogeneous *PTMC* materials targeted for biocompatible applications.

6. Funding

This project was funded by an Aalto University postdoctoral researcher project in synthesis of novel biopolymers (Finland) and by the Centre National de la Recherche Scientifique CNRS (France). The authors declare no conflict of interests.

7. Acknowledgements

This work made use of Aalto University Bioeconomy Facilities. The authors are deeply grateful towards Cédric Lorthioir for sharing the optimized *DQ* ^{1}H Solid State NMR pulse sequence used in this work and towards Paul Sotta for fruitful discussions.

8. Supplementary Information

Supplementary Information available: Equation SI.1; DQ ^1H NMR I_{ref}, I_{DQ}, $I_{ref} - I_{DQ}$, and I_{def} signals obtained for *3k Bulk* PTMC at T_α + 90°C. The contribution from defects I_{def} was fitted from the $I_{ref} - I_{DQ}$ signal and its fraction w_{DEF} was calculated by extrapolating the fit to $\tau_{DQ} = 0$; I_{nDQ} ^1H NMR signals obtained for *3k Bulk PTMC* at various temperatures and normalized according to Equation SI.1; I_{nDQ} ^1H NMR experimental signal obtained for *18k Bulk* PTMC at T_α + 90°C fitted with Equation 5; Typical ^1H NMR spectra for a *PTMC* oligomer and macromer; D_{res} values obtained by *DQ* ^1H NMR measurements as a function of DMA v_C crosslink densities calculated from the *affine* model for all studied *Bulk* and *Solvent-cast PTMC* networks. Percentages correspond to macromer *wt*%. Dashed lines are linear fits and act as a guide for the eyes.

References

[1] K. Zhu, R. Hendren, K. Jensen, C. Pitt, Synthesis, properties, and biodegradation of poly (1,3-trimethylene carbonate), Macromolecules 24 (1991) 1736–1740.

[2] A.-C. Albertson, M. Sjoling, Homopolymerization of 1,8dioxan-2-one to high molecular weight poly(trimethylene carbonate), J. Macromol. Sci. 29 (1) (1992) 43–54. doi:10.1080/10101329208054106.

[3] A.-C. Albertson, M. Eklund, Influence of molecular structure on the degradation mechanism of degradable polymers: In vitro degradation of poly(trimethylene carbonate), poly(trimethylene carbonatecocaprolactone), and poly(adipic anhydride), J. Appl. Polym. Sci. 57 (1) (1995) 87–103. doi:10.1002/app.1995.070570109.

[4] H. Wang, J. H. Dong, K. Y. Qiu, Synthesis and characterization of abatype block copolymer of poly(trimethylene carbonate) with poly(ethylene glycol): Bioerodible copolymer, J. Polym. Sci. Part A: Polym. Chem. 36 (5) (2000) 695–702. doi:10.1002/(SICI)1099-0518(19980415)36:5<695::AID-POLA3>3.0.CO;2-L.

[5] U. Edlund, A.-C.Albertsson, S.K.Singh, I.Fogelberg, B.O.Lundgren, Sterilization, storage stability and in vivo biocompatibility of poly(trimethylene carbonate)/poly(adipic anhydride) blends, Biomaterials 21 (9) (2000) 945–955. doi:10.1016/S0142-9612(99)00268-9.

[6] A. Pêgo, M. V. Luyn, L. Brouwer, P. van Wachem, A. Poot, D. Grijpma, J. Feijen, In vivo behavior of poly(1,3trimethylene carbonate) and copolymers of 1,3trimethylene carbonate with d,llactide or caprolactone: Degradation and tissue response, J. Biomed. Mater. Res. 67A (2003) 1044–1054. doi:10.1002/jbm.a.10121.

[7] Y. Zhang, R. xi Zhuo, Synthesis and drug release behavior of poly (trimethylene carbonate)poly (ethylene glycol)poly (trimethylene carbonate) nanoparticles, Biomaterials 26 (14) (2005) 2751–2760. doi:10.1021/la902786t.

[8] Z. Zhang, D. W. Grijpma, J. Feijen, Thermo-sensitive transition of monomethoxy poly(ethylene glycol)-block-poly(trimethylene carbonate) films to micellar-like nanoparticles, J. Control. Release 112 (1) (2006) 57–63. doi:10.1016/j.jconrel.2006.01.010.

[9] W. J. Habraken, Z. Zhang, J. G. Wolke, D. W. Grijpma, A. G.Mikos, J. Feijen, J. A.Jansen, Introduction of enzymatically degradable poly(trimethylene carbonate) microspheres into an injectable calcium phosphate cement, Biomaterials 29 (16) (2008) 2464–2476. doi:10.1016/j.biomaterials.2008.02.012.

[10] C. Sanson, C. Schatz, J.-F. L. Meins, A. Brûlet, A. Soum, S. Lecommandoux, Biocompatible and biodegradable poly(trimethylene carbonate)-b-poly(l-glutamic acid) polymersomes: Size control and stability, Langmuir 26 (4) (2010) 2751–2760. doi:10.1021/la902786t.

[11] C. Sanson, J.-F. L. Meins, C. Schatz, A. Soum, S. Lecommandoux, Temperature responsive poly(trimethylene carbonate)-block-poly(l-glutamic acid) copolymer: polymersomes fusion and fission, Soft Matter 6 (2010) 1722–1730. doi:10.1039/B924617G.

[12] R. Chapanian, B. Amsden, Combined and sequential delivery of bioactive vegf165 and hgf from poly (trimethylene carbonate) based photo-cross-linked elastomers, J. Control. Release 143 (2010) 53–63. doi:10.1016/j.jconrel.2009.11.025.

[13] X. Jiang, H. Xin, J. Gu, X. Xu, W. Xia, S. Chen, Y. Xie, L. Chen, Y. Chen, X. Sha, X. Fang, Solid tumor penetration by integrin-mediated pegylated poly(trimethylene carbonate) nanoparticles loaded with paclitaxel, Biomaterials 34 (6) (2013) 1739–1746. doi:10.1016/j.biomaterials.2013.09.094.

[14] X. Jiang, H. Xin, Q. Ren, J. Gu, L. Zhu, F. Du, C. Feng, Y. Xie, X. Sha, X. Fang, Nanoparticles of 2-deoxy-d-glucose functionalized poly(ethylene glycol)-co-poly(trimethylene carbonate) for dual-targeted drug delivery in glioma treatment, Biomaterials 35 (1) (2014) 518–529. doi:10.1016/j.biomaterials.2013.09.094.

[15] K. Fukushima, Poly(trimethylene carbonate)-based polymers engineered for biodegradable functional biomaterials, Biomater. Sci. 4 (2016) 9–24. doi:10.1039/C5BM00123D.

[16] S. Schüller-Ravoo, J. Feijen, D. Grijpma, Flexible, elastic and tear-resistant networks prepared by photo-crosslinking poly(trimethylene carbonate) macromers, Acta Biomaterialia 8 (2012) 3576–3585. doi:10.1016/j.actbio.2012.06.004.

[17] B. van Bochove, G. Hannink, P. Buma, D. Grijpma, Preparation of designed poly(trimethylene carbonate) meniscus implants by stereolithography: Challenges in stereolithography, Macromolecular Biosience 16 (2016) 1853–1863. doi:10.1002/mabi.201600290.

[18] E. Zant, D. Grijpma, Tough biodegradable mixed-macromer networks and hydrogels by photo-crosslinking in solution, Acta Biomaterialia 31 (2016) 80–88. doi:10.1016/j.actbio.2015.12.014.

[19] B. van Bochove, S. Schüller-Ravoo, D. W. Grijpma, Photo-crosslinked elastomeric bimodal poly(trimethylene carbonate) networks, Macromol. Mater. Eng. (2019) 1800623doi:10.1002/mame.201800623.

[20] M. Geven, V. Varjas, L. Kamer, X. Wang, J. Peng, D. Eglin, D. Grijpma, Fabrication of patient specific composite orbital floor implants by stereolithography, Polym. Advan. Technol. 26 (2015) 1433–1438. doi:10.1002/pat.3589.

[21] S. Schüller-Ravoo, E. Zant, J. Feijen, D. Grijpma, Preparation of a designed poly(trimethylene carbonate) microvascular network by stereolithography, Adv. Healthc. Mat. 3 (2014) 2004–2011. doi:10.1002/adhm.201400363.

[22] B. Amsden, Curable, biodegradable elastomers: emerging biomaterials for drug delivery and tissue engineering, Soft Matter 3 (2007) 1335–1348. doi:10.1039/B707472G.

[23] T. L. Smith, Strength of elastornersa perspective, Polym. Eng. Sci. 17 (3) (1977) 129–143. doi:10.1002/pen.760170302.

[24] M. S. Hoo Fatt, L. Chen, A. A. Al-Quraishi, Fracture parameters for natural rubber under dynamic loading, Strain 47 (s1) (2011) e505–e518. doi:10.1111/j.1475-1305.2009.00647.x.

[25] J. K. Premachandra, J. E. Mark, Effects of dilution during crosslinking on strain-induced crystallization in cis-1,4-polyisprene networks. i. experimental results, J. Macromol. Sci. A 39 (4) (2002) 287–300. doi:10.1081/MA-120003280.

[26] R. M. Johnson, J. E. Mark, Properties of poly(dimethylsiloxane) networks prepared in solution, and their use in evaluating the theories of rubberlike elasticity, Macromolecules 5 (1) (1972) 41–45. doi:10.1021/ma60025a011.

[27] J. E. Mark, Improved elastomers through control of network chain-length distributions, Rubber Chem. Technol. 72 (3) (1999) 465–483. doi:10.5254/1.3538814.

[28] K. Urayama, Network topology mechanical properties relationships of model elastomers, Polym. J. 40 (8) (2008) 669–678.

[29] V. Vasiliev, L. Rogovina, G. Slonimsky, Dependence of properties of swollen and dry polymer networks on the conditions of their formation in solution, Polymer 26 (11) (1985) 1667 – 1676. doi:10.1016/0032-3861(85)90284-8.

[30] B. G. Amsden, G. Misra, F. Gu, H. M. Younes, Synthesis and characterization of a photo-cross-linked biodegradable elastomer, Biomacromolecules 5 (6) (2004) 2479–2486. doi:10.1021/bm049578h.

[31] F. P. W. Melchels, A. H. Velders, J. Feijen, D. W. Grijpma, Photo-cross-linked poly(dl-lactide)-based networks. structural characterization by hr-mas nmr spectroscopy and hydrolytic degradation behavior, Macromolecules 43 (20) (2010) 8570–8579. doi:10.1021/ma1011705.

[32] J.-L. Hallary, F. Lauprêtre, L. Monnerie (Eds.), Polymer Materials, Macroscopic Properties and Molecular Interpetrations, John Wiley & Sons, Hoboken, 2010.

[33] M. C. Tanzi, S. Farè (Eds.), Characterization of Polymeric Biomaterials, Elsevier, Cambridge, 2017.

[34] I. Prigogine, R. S. A. (Eds.), Advances in Chemical Physics Vol. LXVI, John Wiley & Sons, New York, 1987.

[35] D. D. Laws, H.-M. L. Bitter, A. Jerschow, Solid-state nmr spectroscopic methods in chemistry, Angew. Chem. Int. Ed. 41 (2002) 3096–3129.

[36] K. Schmidt-Rohr, H. W. Spiess (Eds.), Multidimensional Solid-State NMR and Polymers, Academic Press, London, 2005.

[37] G. A. Webb (Ed.), Modern Magnetic Resonance, Springer, Cham, 2006.

[38] H. Y. Carr, E. M. Purcell, Effects of diffusion on free precession in nuclear magnetic resonance experiments, Phys. Rev. 94 (1954) 630–638. doi:10.1103/PhysRev.94.630.

[39] S. Meiboom, D. Gill, Modified spinecho method for measuring nuclear relaxation times, Rev. Sci. Instrum. 29 (1958) 688–691. doi:10.1063/1.1716296.

[40] J. P. Cohen-Addad, Effect of the anisotropic chain motion in molten polymers: The solidlike contribution of the nonzero average dipolar coupling to nmr signals. theoretical description, J. Chem. Phys. 60 (1974) 2040–2053. doi:10.1063/1.1681380.

[41] J. P. Cohen-Addad, C. Schmit, Nuclear magnetic resonance approach to fractal chain structure in molten polymers and gels: Characterization method of the spin-system response, Polymer 29 (1988) 883–893. doi:032-3861/88/050883-11.

[42] P. Sotta, C. Fülber, D. E. Demco, B. Blümich, H. W. Spiess, Effect of residual dipolar interactions on the nmr relaxation in cross-linked elastomers, Macromolecules 29 (1996) 6222–6230. doi:10.1021/ma960141e.

[43] P. Sotta, Local order and induced orientation in pdms model networks, studied by ^2h nmr, Macromolecules 31 (12) (1998) 3872–3879. doi:10.1021/ma970994m.

[44] F. Mellinger, M. Wilhelm, P. Belik, H. Schwind, H. W. Spiess, Quantitative determination of dynamic heterogeneities in coreshell latices by ^1H solid-state nmr, Macromol. Chem. Phys. 200 (1999) 2454–2460. doi:1022-1352/99/11112454.

[45] R. Fechete, D. Demco, B. Blümich, U. Eliav, G. Navon, Anisotropy of collagen fiber orientation in sheep tendon by ^1H double-quantum-filtered nmr signals, J. Magn. Res. 162 (2003) 166–175. doi:10.1016/S1090-7807(02)00200-8.

[46] Y.-S. Yen, A. Pines, Multiple-quantum nmr in solids, J. Chem. Phys. Part II 78 (1983) 3579–3582.

[47] J. Baum, M. Munowitz, A. N. Garroway, A. Pines, Multiplequantum dynamics in solid state nmr, J. Chem. Phys. 83 (1985) 2015–2025. doi:10.1063/1.449344.

[48] J. Baum, A. Pines, Nmr studies of clustering in solids, J. Am. Chem. Soc. 108 (1986) 7447–7454.

[49] K. Saalwächter, P. Ziegler, O. Spyckerelle, B. Haidar, A. Vidal, J. U. Sommer, ^1H multiple-quantum nuclear magnetic resonance investigations of molecular order distributions in poly(dimethylsiloxane) networks: Evidence for a linear mixing law in bimodal systems, J. Chem. Phys. 119 (2003) 3468–3482. doi:10.1063/1.1589000.

[50] K. Saalwächter, ^1H multiple-quantum nuclear magnetic resonance investigations of molecular order in polymer networks. ii. intensity decay and restricted slow dynamics, J. Chem. Phys. 120 (2004) 454–464. doi:10.1063/1.1630561.

[51] K. Saalwächter, F. Kleinschmidt, J.-U. Sommer, Swelling heterogeneities in end-linked model networks: A combined proton multiple-quantum nmr and computer simulation study, Macromolecules 37 (2004) 8556–8568. doi:10.1021/ma048803k.

[52] K. Saalwächter, B. Herrero, M. A. López-Manchado, Chain order and cross-link density of elastomers as investigated by proton multiple-quantum nmr, Macromolecules 38 (2005) 9650–9660. doi:10.1021/ma051238g.

[53] K. Saalwächter, Proton multiple-quantum nmr for the study of chain dynamics and structural constraints in polymeric soft materials, Prog. Nucl. Magn. Reson. Spectrosc. 51 (2007) 1–35.

[54] W. Chassé, S. Schlögl, G. Riess, K. Saalwächter, Inhomogeneities and local chain stretching in partially swollen networks, Soft Matter 9 (2013) 6943–6954. doi:10.1039/c3sm50195g.

[55] M. Mansilla, J. Valentín, M. López-Manchado, A. González-Jiménez, A. Marzocca, Effect of entanglements in the microstructure of cured nr/sbr blends prepared by solution and mixing in a two-roll mill, E. Polym. J. 81 (2016) 365–375. doi:10.1016/j.eurpolymj.2016.06.023.

[56] C. Lorthioir, S. Randriamahefa, B. Deloche, Some aspects of the orientational order distribution of flexible chains in a diblock mesophase, J. Chem. Phys. 139 (2013) 224903. doi:10.1063/1.4838375.

[57] C. Lorthioir, B. Deloche, Heterogeneous behavior of free chain-ends in a lamellar diblock copolymer: segmental dynamics and ordering, as probed by ^2H solid-state nmr, Colloid Polym. Sci. 292 (2014) 1841–1851.

[58] K. Saalwächter, A. Heuer, Chain dynamics in elastomers as investigated by proton multiple-quantum nmr, Macromolecules 39 (2006) 3291–3301. doi:10.1021/ma052567b.

[59] F. V. Chávez, K. Saalwächter, Time-domain nmr observation of entangled polymer dynamics: Analytical theory of signal functions, Macromolecules 44 (2011) 1560–1569. doi:10.1021/ma102571u.

[60] M. Martin-Gallego, A. González-Jiménez, R. Verdejo, M. A. López-Manchado, J. L. Valentín, Epoxy resin curing reaction studied by proton multiple-quantum nmr, J. Polym. Sci. Part B Polym. Phys. 53 (2015) 1324–1332. doi:10.1002/polb.23767.

[61] E. Gjersing, S. Chinn, J. R. Giuliani, J. Herberg, R. S. Maxwell, E. Eastwood, D. Bowen, T. Stephens, Investigation of network heterogeneities in filled, trimodal, highly functional pdms networks by ^1H multiple quantum nmr, Macromolecules 40 (2007) 4953–4962. doi:10.1021/ma0620924.

[62] A. Vieyres, R. Pérez-Aparicio, P.-A. Albouy, O. Sanseau, K. Saalwächter, D. R. Long, P. Sotta, Sulfur-cured natural rubber elastomer networks: Correlating cross-link density, chain orientation, and mechanical response by combined techniques, Macromolecules 43 (2013) 889–899. doi:10.1021/ma302563z.

[63] A. Rios de Anda, P. Sotta, T. Modjinou, V. Langlois, D.-L. Versace, E. Renard, Multiscale structural characterization of biobased diallyl-eugenol polymer networks, Macromolecules 53 (6) (2020) 2187–2197. doi:10.1021/acs.macromol.9b02280.

[64] J. R. Giuliani, E. L. Gjersing, S. C. Chinn, T. V. Jones, T. S. Wilson, C. T. Alviso, J. L. Herberg, M. A. Pearson, R. S. Maxwell, Thermal degradation in a trimodal poly(dimethylsiloxane) network studied by 1h multiple quantum nmr, J. Phys. Chem. B 111 (2007) 12977–12984. doi:10.1021/jp075840f.

[65] B. Gabrielle, C. Lorthioir, F. Lauprêtre, Thermal aging of interfacial polymer chains in ethylene-propylene-diene terpolymer/aluminum hydroxide composites: Solid-state nmr study, J. Phys. Chem. B 115 (2011) 12392–12400. doi:10.1021/jp207084j.

[66] B. van Bochove, S. Spoljaric, J. Seppälä, P. Sotta, A. Rios de Anda, Multiscale characterization of biocompatible poly(trimethylene carbonate) photoreticulated networks by coupling of dma and multiple quanta ^1H solid state nmr measurements, ACS Appl. Polym. Mat. 1 (7) (2019) 1811–1820. doi:10.1021/acsapm.9b00338.

[67] T. Pirvu, S. B. Blanquer, L. M. Benneker, D. W. Grijpma, R. G. Richards, M. Alini, D. Eglin, S. Grad, Z. Li, A combined biomaterial and cellular approach for annulus fibrosus rupture repair, Biomaterials 42 (2015) 11–19. doi:https://doi.org/10.1016/j.biomaterials.2014.11.049.

[68] J. J. Rongen, B. van Bochove, G. Hannink, D. W. Grijpma, P. Buma, Degradation behavior of, and tissue response to photo-crosslinked poly(trimethylene carbonate) networks, J. Biomed. Mater. Res. A 104 (11) (2016) 2823–2832. doi:10.1002/jbm.a.35826.

[69] E. Bat, B. H. Kothman, G. A. Higuera, C. A. [van Blitterswijk], J. Feijen, D. W. Grijpma, Ultraviolet light crosslinking of poly(trimethylene carbonate) for elastomeric tissue engineering scaffolds, Biomaterials 31 (33) (2010) 8696–8705. doi:https://doi.org/10.1016/j.biomaterials.2010.07.102.

[70] S. Schller-Ravoo, S. M. Teixeira, J. Feijen, D. W. Grijpma, A. A. Poot, Flexible and elastic scaffolds for cartilage tissue engineering prepared by stereolithography using poly(trimethylene carbonate)-based resins, Macromol. Biosci. 13 (12) (2013) 1711–1719. doi:10.1002/mabi.201300399.

[71] O. Guillaume, M. Geven, C. Sprecher, V. Stadelmann, D. Grijpma, T. Tang, L. Qin, Y. Lai, M. Alini, J. de Bruijn, H. Yuan, R. Richards, D. Eglin, Surface-enrichment with hydroxyapatite nanoparticles in stereolithography-fabricated composite polymer scaffolds promotes bone

repair, Acta Biomaterialia 54 (2017) 386–398. doi:https://doi.org/10.1016/j.actbio.2017.03.006.

[72] O. Guillaume, M. A. Geven, V. Varjas, P. Varga, D. Gehweiler, V. A. Stadelmann, T. Smidt, S. Zeiter, C. Sprecher, R. R. Bos, D. W. Grijpma, M. Alini, H. Yuan, G. R. Richards, T. Tang, L. Qin, L. Yuxiao, P. Jiang, D. Eglin, Orbital floor repair using patient specific osteoinductive implant made by stereolithography, Biomaterials 233 (2020) 119721. doi:https://doi.org/10.1016/j.biomaterials.2019.119721.

[73] A. Rios de Anda, L.-A. Fillot, D. Long, P. Sotta, Influence of the amorphous phase molecular mobility on impact and tensile properties of polyamide 6,6, J. Appl. Polym. Sci. 133 (2016) 43457. doi:10.1002/app.43457.

[74] P. J. Flory (Ed.), Principles of Polymer Chemistry, Cornell University Press, Ithaca and London, 1953.

[75] H. M. James, E. Guth, Statistical thermodynamics of rubber elasticity, J. Chem. Phys. 21 (1953) 1039–1049. doi:10.1063/1.1699106.

[76] R. Pérez-Aparicio, A. Vieyres, P.-A. Albouy, O. Sanseau, L. Vanel, D. R. Long, P. Sotta, Reinforcement in natural rubber elastomer nanocomposites: Breakdown of entropic elasticity, Macromolecules 46 (2013) 8964–8972. doi:10.1021/ma401910c.

[77] L. D. Landau, E. M. Lifshitz (Eds.), Theory of Elasticity, Pergamon Press, Oxford, 1970.

[78] L. Treloar (Ed.), The Physics of Rubber Elasticity, Claredon Press, Oxford, 1975.

Graphical Abstract

Multiscale Structural Characterization of Biocompatible Poly(trimethylene carbonate) Networks Photo-cross-linked in a Solvent

Bas van Bochove, Steve Spoljaric, Jukka Seppälä, Agustín Rios de Anda

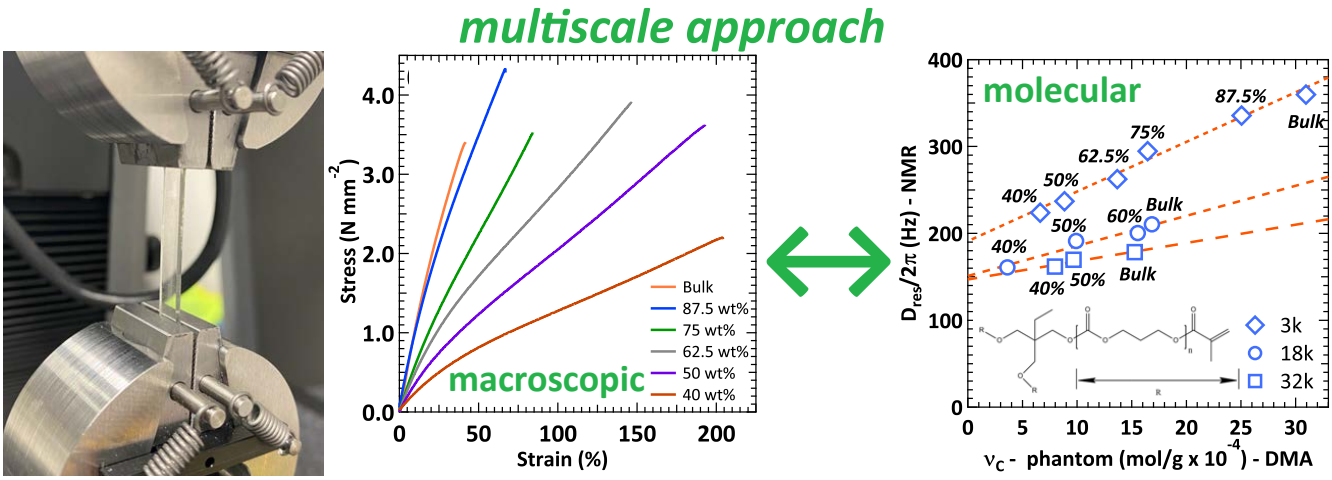

multiscale approach

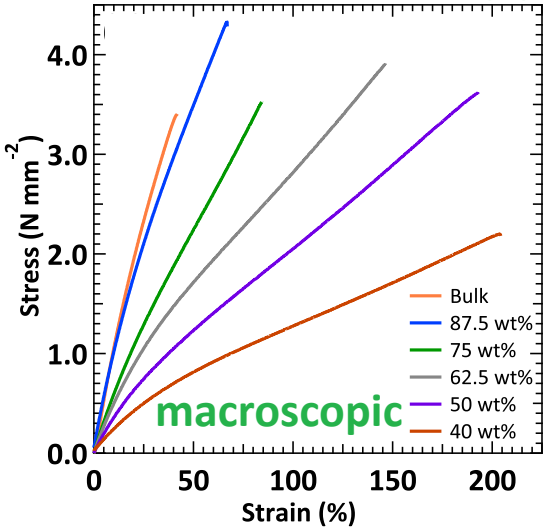

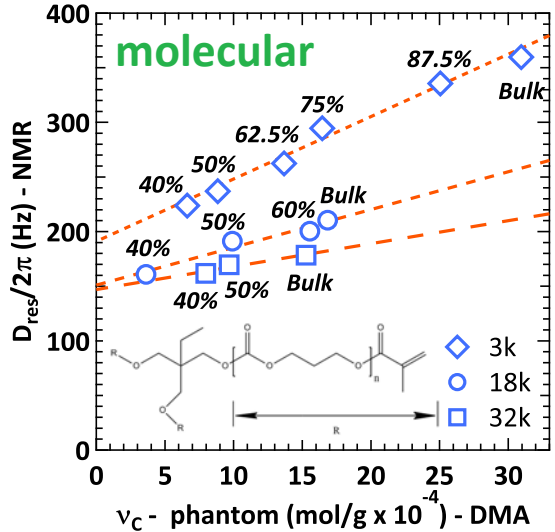

multiscale approach